Temperature and pressure dependence of the reaction of OH and CO: Master equation modeling on a high-level potential energy surface

ARTICLE *in* INTERNATIONAL JOURNAL OF CHEMICAL KINETICS · SEPTEMBER 2003

Impact Factor: 1.52 · DOI: 10.1002/kin.10144

3 AUTHORS, INCLUDING:

Juan Pablo Senosiain
Laboratorios Senosiain
18 PUBLICATIONS **595** CITATIONS

Temperature and Pressure Dependence of the Reaction of OH and CO: Master Equation Modeling on a High-Level Potential Energy Surface

JUAN P. SENOSIAIN,[1] CHARLES B. MUSGRAVE,[1,2] DAVID M. GOLDEN[3]

[1]*Department of Materials Science and Engineering, Stanford University, Stanford, California* 94305
[2]*Department of Chemical Engineering, Stanford University, Stanford, California* 94305
[3]*Department of Mechanical Engineering, Stanford University, Stanford, California* 94305

Received 16 December 2002; accepted 8 May 2003

DOI 10.1002/kin.10144

ABSTRACT: The temperature and pressure dependence of the reaction of OH + CO has been modeled using the (energy-resolved) master equation and RRKM theory. These calculations are based on the coupled-cluster potential energy surface of Yu and co-workers (Chem Phys Lett 349, 547–554, 2001). As is well known, this reaction shows a strong non-Arrhenius behavior at moderate and low temperatures because of the stabilization of the HOCO intermediate. Kinetic simulations are in excellent agreement with experiments at temperatures above 300 K, but the agreement is only modest at temperatures below 250 K. Our calculations indicate that the contribution of tunneling to the rate constant is marginal, given the small energy difference between the transition states corresponding to formation and decomposition of the HOCO intermediate. Parametric fits to the calculated rate constants are provided for modeling purposes. © 2003 Wiley Periodicals, Inc. Int J Chem Kinet 35: 464–474, 2003

INTRODUCTION

The reaction of carbon monoxide with hydroxyl radicals is of vital importance for combustion and atmospheric processes. In the case of hydrocarbon combustion, this is the main mechanism for converting CO into CO_2 and is responsible for a major fraction of the energy release. In the lower atmosphere, this reaction is implicated in smog formation by regulating the concentration of hydroxyl radicals that play a crucial role in NO_x and HO_x chemical cycles.

Because of its importance and its unusual temperature and pressure behavior, this system has inspired a large body of work, both theoretical and experimental.

Correspondence to: David M. Golden; e-mail: david.golden@stanford.edu.

Contract grant sponsor: NASA Upper Atmosphere Research Program.
Contract grant number: NAG 2-1397-1.

The temperature dependence presents two regimes with markedly different activation energies, with a transition around 500 K.

In 1964 Ung and Back postulated the existence of the hydroxyoxomethyl radical (HOCO) as an intermediate in the addition of OH and CO [1]. Dryer et al. [2] showed that transition state theory can predict the strong non-Arrhenius behavior of this reaction if the activation barrier is close to zero. The role of the collisional stabilization of HOCO and the complicated temperature and pressure dependence of this reaction was studied by Smith and Zellner [3] and Smith [4], who proposed the general reaction mechanism illustrated in Scheme 1.

The currently accepted reaction mechanism consists of an OH + CO association step forming *trans*-HOCO, followed by facile cis–trans isomerization and finally a decomposition step to H + CO_2. At moderate pressures, stabilization of HOCO intermediates competes with the decomposition channel and the back reaction to OH + CO.

It is interesting to note that when OH and CO react in air, both reaction channels eventually lead to the same final products, namely HO_2 + CO_2.

The existence of HOCO and DOCO has been confirmed with matrix-isolation techniques [5], photoionization mass spectroscopy [6,7], and ultrafast laser spectroscopy [8] of the OH radical produced in the reverse reaction of H + CO_2. The vibrational and rotational spectra of these radicals have been characterized [9].

The heat of formation of the HOCO intermediates, relative to the OH + CO entrance channel, is of some importance for kinetic calculations in the falloff regime. Until recently, the accepted well depth of the *trans*-HOCO intermediate was presumed to be 35.4 kcal/mol below the OH + CO level, based on a $\Delta_f H^0_{298\,K}$ (*trans*-HOCO) = −52.5 kcal/mol from photoionization studies [7]. However, more recent measurements [6] have set an upper limit of $\Delta_f H^0_{298K}$ (*trans*-HOCO) > −46.5 kcal/mol, implying a *trans*-HOCO well depth of 28.9 kcal/mol at most [10]. (The heat of formation (at 0 K) of the hydroxyl radical has recently been revised to a value 0.5 kcal/mol lower than previously thought.) This is consistent with lower well depths of more recent ab initio calculations [11–13]. For comparison purposes, energies of the *trans*-HOCO intermediate and the key transition states obtained with different quantum chemistry methods are compiled in Table I.

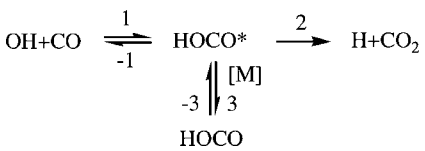

Scheme 1

The formation of hydrogen-bound OHCO and OHOC complexes as intermediates to formation of HOCO was first predicted by Frost and co-workers [19]. The semiempirical potential energy surface (PES) calculated by Kudla et al. [20] contains minima corresponding to OHCO and OHOC complexes. Later these loosely bound complexes were observed spectroscopically by Lester and co-workers [21], but their role in the kinetics of OH + CO complexes remains unclear.

The reaction of OH with CO has been the subject of several theoretical and experimental investigations. Thermal reaction rate constants for this reaction have been measured at temperatures as high as 2800 K [22,23] and as low as 80 K [17,19,24]. For a concise summary of earlier work, see Refs. [25] and [26].

One of the earlier first-principle studies of this surface was done by Feller et al. [27] who carried out configuration interaction (CI) calculations on the HCO_2 radical and found transition state structures for the 1,2 hydrogen shift and for decomposition to H + CO_2. McLean and Ellinger [28] studied the cis and trans isomers of HOCO, using CI with localized basis sets and discovered that electron correlation is necessary to correctly describe the relative stability of these two isomers. Aoyagi and Kato [14] performed MCSCF and MRD-CI calculations and studied the effects of tunneling in the decomposition reaction. They calculated a transition state for HOCO decomposition that was 18.4 kcal/mol above the entrance channel, and concluded that the observed weak temperature dependence was due to tunneling. A semiempirical characterization of the multidimensional PES has been done by Schatz and co-workers [20,29,30]. More recently, this PES has been studied by Zhu and co-workers [13] using the G2M method, and by Yu et al. [11] with coupled cluster and extrapolation techniques. In addition, a number of dynamics studies have been performed on this system, including quasi-classical trajectory calculations [15,31], quantum dynamics calculations [32], and a recent investigation using quantum-dressed classical mechanics [33].

Early attempts [4,19,34,35] to model the reaction of CO and OH radicals based on RRKM theory and a pseudostrong collision approximation failed to predict the near-temperature-independent rate constant below 500 K. Three more recent studies have modeled this reaction, claiming to fit experimental rate coefficients to temperatures down to 80 K. Fulle et al. [17] and Troe [36] performed E- and J-resolved RRKM calculations with a pseudostrong collision energy transfer model. They fit high- and low-pressure rate coefficients to

Table I Comparison of Selected Stationary Points of OH + CO PES[a]

Author	Method	*trans*-TS1	*cis*-TS2	*trans*-HOCO
Aoyagi and Kato[b] [14]	MCSCF	15.8	31.5	0.4
	MRD-CI	5.2	18.7	−12.0
Schatz et al. [15]	Semiempirical	−1.15	3	−37.12
Golden et al. [16]	Optimization	1.07	0.6	−34.48
Duncan and Miller [12]	G3	0	0	−24.3
	CBS-QB3	0	1.1	−25.4
Zhu et al. [13]	G2M	0.8	2.3	−23.9
Yu et al. [11]	FCC (extrapolated)	0.57	1.03	−25.34
Fulle et al. [20]	Experimental	0.43	TS1 ± 0.17	−30.83
Ruscic et al. [7]	Photoionization			−28.9

[a] Zero-point corrected energies (kcal/mol) relative to OH + CO.
[b] Experimental frequencies of OH and CO from Ref. [18] used for zero-point energy corrections.

optimize the PES of Kudla et al. [15], and reported that the two competing channels for HOCO dissociation (OH + CO and H + CO_2) are responsible for the observed biexponential decay of OH. Zhu et al. [13] performed an RRKM/master equation study based on their G2M surface, and attributed the unusually high low-temperature rate coefficients to a pronounced tunneling effect. They noted, however, that the magnitude of Wigner tunneling corrections is very sensitive to the imaginary frequency of TS2, which varies greatly depending on the method of calculation.

In 1998 Golden and co-workers [16] used statistical methods to fit the existing experimental data, optimizing the controlling barriers and the vibrational frequencies of *trans*-TS1 from Ref. [15]. This fit yielded an optimized energy of *cis*-TS2 slightly below the entrance channel. The objective of the present study is to generate a physically based model that reproduces the large body of experimental data and allows for reliable extrapolations to unknown conditions.

CALCULATION OF THERMAL RATE CONSTANTS

Rate calculations presented in this paper were done using the PES of Yu and co-workers [11]. This surface is based on ab initio calculations done at the CCSD(T)/cc-pvTZ level and extrapolated to the infinite coupled-cluster limit and complete basis set. The density of states of the stable compounds and the sum of states of transition states were calculated with the Stein–Rabinovitch "exact count" method [37], using geometries and frequencies from Ref. [11]. All the modes were treated within the rigid-rotor harmonic oscillator approximation except for the out-of-plane torsion of *trans*-TS1 that was modeled as a hindered rotor. Microcanonical reaction rates were calculated using RRKM theory and solving the two coupled master equations corresponding to the trans and cis forms of HOCO intermediates:

$$\frac{\mathrm{d}y_i(E',t)}{\mathrm{d}t}\,\mathrm{d}E' = \int_0^\infty [R(E' \leftarrow E)\,\mathrm{d}E'\,y_i(E,t)]\,\mathrm{d}E - \int_0^\infty [R(E \leftarrow E')\,\mathrm{d}E'\,y_i(E',t)]\,\mathrm{d}E + \sum [k_{\mathrm{in}}(E') - k_{\mathrm{out}}(E')]\,y_i(E',t)\,\mathrm{d}E'$$

where $y_i(E',t)\,\mathrm{d}E'$ is the instantaneous concentration of the i-th well (i.e. i = *trans*-HOCO, *cis*-HOCO) with vibrational energy in the range E' to $E' + \mathrm{d}E'$, k_{in} and k_{out} are reaction rate constants producing and consuming y_i, respectively, and $R(E \leftarrow E')$ is the rate coefficient of vibrational energy transfer (VET) from E' to E. The latter can be written as the product of the inelastic collision frequency and the "collision step-size distribution," $P(E \leftarrow E')$ [38]*:

$$R(E \leftarrow E') = \omega P(E \leftarrow E')$$

The inelastic collision frequency (ω) can be written as the product of the bath gas concentration, [M], and the bimolecular collision rate constant k_{coll}. (It should be noted that these two quantities are intrinsically related to each other, and the above relationship holds only when the omega is equal to the inelastic rate coefficient.) The latter quantity was calculated assuming Lennard–Jones collisions, with parameters $\sigma = 3.94$ Å and $\varepsilon = 201$ K for the HOCO system (by analogy to

*Note that $P(E \leftarrow E')$ and ω are intrinsically related, and this equation only holds when ω is the inelastic collision rate.

CO_2). These parameters are in close agreement with the MP2 estimation of Zhu et al. (op cit). It is convenient to express the probability for deactivating collisions with the simple "exponential down" model:

$$P(E \leftarrow E') \propto \exp\left(-\frac{E'-E}{\alpha_0}\right) \quad E' > E$$

where the energy transfer parameter α_0 is assumed to be independent of temperature but distinct for each bath gas. The step-size distribution for activating collisions were calculated from detailed balance. Although considerable effort has been directed to the characterization of VET processes (for a recent review see Ref. [38]), the experimental data for energy transfer parameters are far from complete and often contain large uncertainties. For this reason, we obtained α_0 for each bath gas by fitting experimental falloff rates.

All thermochemical and master equation calculations were performed using the Multiwell [39] collection of programs, which is based on Gillespie's Monte Carlo algorithm [40] for solving the master equation. For the pressure and temperature ranges considered, quasi-steady-state conditions were achieved within 200 collisions or less, and in most cases 10^5 trials were sufficient to obtain 0.1% accuracy in the rate coefficients.

Based on the mechanism presented in Scheme 1, the bimolecular rate constant for the association of OH and CO is given by

$$k_{\mathrm{bi}}^{\mathrm{assoc}}(E) = \frac{k_1(E)k_3'(E)[\mathrm{M}]}{k_{-1}(E)+k_2(E)+k_3'(E)[\mathrm{M}]}$$

when the collisional reactivation of the intermediates is neglected. Under low-pressure conditions, the association channel can be expressed as a pseudo-first-order reaction:

$$k_0^{\mathrm{assoc}}(E) = \left(\frac{k_1(E)k_3'(E)}{k_{-1}(E)+k_2(E)}\right)[\mathrm{M}]$$

Following the formalism of Troe [41], the reduced reaction association rate coefficient can be written as

$$k_{\mathrm{r}}^{\mathrm{assoc}}(E) = \frac{k^{\mathrm{assoc}}(E)}{k_\infty^{\mathrm{assoc}}(E)} = \frac{P_{\mathrm{r}}^{\mathrm{assoc}}}{1+P_{\mathrm{r}}^{\mathrm{assoc}}} F^{\mathrm{assoc}}\left(P_{\mathrm{r}}^{\mathrm{assoc}}\right)$$

where the reduced pressure ($P_{\mathrm{r}}^{\mathrm{assoc}}$) is the ratio of the low-pressure and high-pressure rate coefficients:

$$P_{\mathrm{r}}^{\mathrm{assoc}} = \frac{k_0^{\mathrm{assoc}}(E)}{k_\infty^{\mathrm{assoc}}(E)} = \frac{k_3'(E)[\mathrm{M}]}{k_{-1}(E)+k_2(E)}$$

and F^{assoc} is an empirical broadening factor.

Conversely, the bimolecular reaction rate for the chemical activation channel leading to $H + CO_2$ products is given by

$$k_{\mathrm{bi}}^{\mathrm{ca}}(E) = \frac{k_1(E)k_2(E)}{k_{-1}(E)+k_2(E)+k_3'(E)[\mathrm{M}]}$$

In the high-pressure limit the rate coefficient for the chemical activation channel is inversely proportional to the pressure:

$$k_\infty^{\mathrm{ca}}(E) = \frac{k_1(E)k_2(E)}{k_3'(E)[\mathrm{M}]}$$

and the reduced rate constant for the chemical activation channel* is best expressed as

$$k_{\mathrm{r}}^{\mathrm{ca}}(E) = \frac{k^{\mathrm{ca}}(E)}{k_0^{\mathrm{ca}}(E)} = \frac{P_{\mathrm{r}}^{\mathrm{ca}}}{1+P_{\mathrm{r}}^{\mathrm{ca}}} F^{\mathrm{ca}}\left(P_{\mathrm{r}}^{\mathrm{ca}}\right)$$

with the reduced pressure in this case given by the ratio

$$P_{\mathrm{r}}^{\mathrm{ca}} = \frac{k_\infty^{\mathrm{ca}}(E)}{k_0^{\mathrm{ca}}(E)} = \frac{k_{-1}(E)+k_2(E)}{k_3'(E)[\mathrm{M}]}$$

The microcanonical rate constant for OH disappearance in the steady-state regime can be written as the sum of the chemical activation and association channels:

$$\begin{aligned} k_{\mathrm{OH+CO}}(E) &= k^{\mathrm{assoc}}(E) + k^{\mathrm{ca}}(E) \\ &= k_1(E)\left(\frac{k_2(E)+k_3'(E)[\mathrm{M}]}{k_{-1}(E)+k_2(E)+k_3'(E)[\mathrm{M}]}\right) \end{aligned}$$

TUNNELING CALCULATIONS

The geometry and intrinsic reaction coordinate (IRC) curve of *cis*-TS2 was calculated using the hybrid DFT method KMLYP [42], with the 6-311+G(d,p) basis set using the Gaussian 98 collection of programs [43]. Frequency calculations were performed every 0.10 bohr $\mathrm{amu}^{1/2}$ along the IRC curve to correct it for zero-point energy (V_a). The vibrationally adiabatic minimum energy pathway $V_a(s)$ of *cis*-TS1 is shown in Fig. 1 for HOCO and DOCO systems. The semiclassical tunneling probability is given by [44]

$$\tau(E) = \exp[-2\theta(E)]$$

*In this paper we use reciprocal definitions of the reduced rate constants and pressures for the association and chemical activation channels. This was done to facilitate the parametric fits of the chemical activation channel.

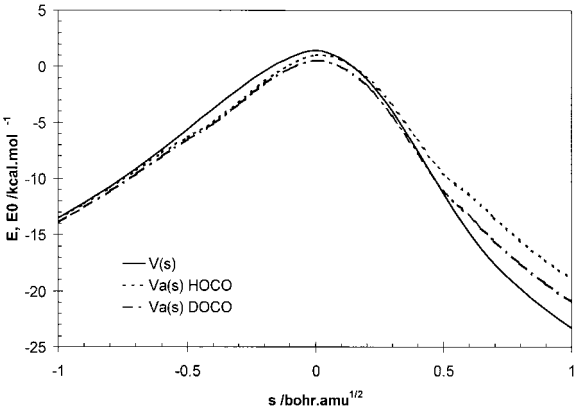

Figure 1 Intrinsic reaction coordinate for reaction 2 (solid line) and vibrationally adiabatic potentials for OH + CO (dashed) and OD + CO (dash-dot).

where $\theta(E)$ is the imaginary action integral:

$$\theta(E) = \frac{1}{\hbar} \int_{s_1(E)}^{s_2(E)} 2\mu_{\text{eff}}(s)[V_a(s) - E]^{1/2}\, ds$$

Within the zero curvature tunneling (ZCT) approximation, the effective mass for tunneling (μ_{eff}) is regarded as independent of the reaction coordinate (s) and equal to the reduced mass (μ_r) [45]. The effect of tunneling was incorporated in the master equation calculations by replacing the sum of states of the transition state in the RRKM expression by the microcanonical tunneling probability, as suggested by Miller [46]:

$$k(E) = \frac{1}{h} \frac{W_T(E')}{\rho(E)}$$

$$W_T(E') = \begin{cases} \tau(E') & E < V_2 \\ W(E') & E \geq V_2 \end{cases}$$

where V_2 is the (zero-point corrected) barrier for reaction 2. To implement this method with the Multiwell program, the energy threshold for reaction 2 was set below V_2 to account for the "tunneling states." In practice, we found that lowering this threshold by 3000 cm^{-1} was enough to capture ca. 90% of the tunneling rate, yet maintaining the arrays within a manageable size.

RESULTS AND DISCUSSION

Temperature Dependence

The temperature dependence of the disappearance of OH at low pressures is shown in Figs. 2 and 3. Although the calculated high-pressure rate coefficients at

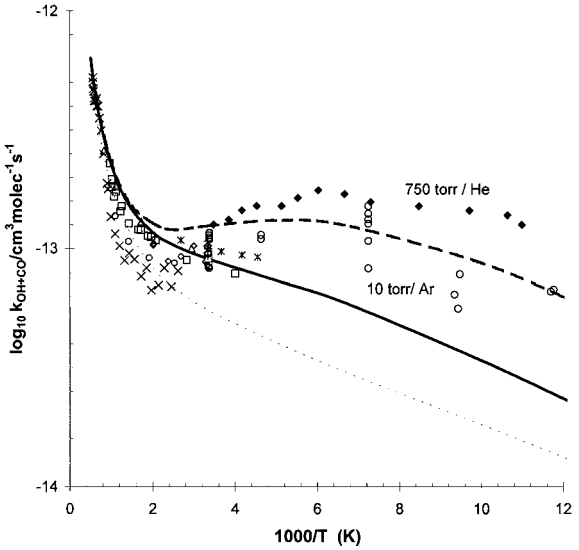

Figure 2 Arrhenius plot of k_{OH+CO} (measuring OH disappearance) at low pressures. ○ Ref. [19] (2–10 torr Ar), ◆ Ref. [17] (750 torr He), △ Ref. [47], □ Ref. [48], ■ Ref. [49], ● Ref. [50], ✱ Ref. [51], ▲ Ref. [52], × Ref. [23], + Ref. [53], ◇ Ref. [54]. Solid and dashed lines represent simulations with 10 torr of Ar and bath gas with 750 torr of He bath gases, respectively, with $E_0(cis\text{-TS2}) = 0.6$ kcal/mol. The dotted line shows the simulation with 10 torr of Ar using $E_0(cis\text{-TS2}) =$ 1.0 kcal/mol.

298 K agree very well with the experimental values of Refs. [17] and [34], the calculated low-pressure rates are too low by ca. 40%. For this reason we adjusted the PES by lowering the energy of TS2 by 0.4 kcal/mol, fitting the experimental low-pressure rate coefficients at 298 K.

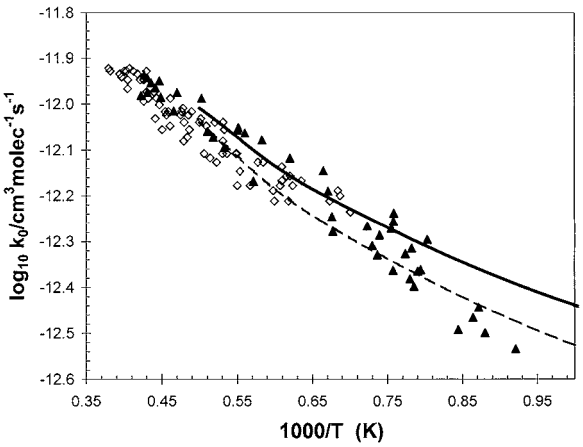

Figure 3 High temperature portion of Fig. 2. Symbols represent experimental data: ▲ Ref. [22], ◇ Ref. [16]. Solid line represents present study: solid line with $E_0(cis\text{-TS2}) = 0.6$ kcal/mol and dashed line with $E_0(cis\text{-TS2}) =$ 1.0 kcal/mol.

Two groups have measured the rate coefficients of the title reaction at temperatures below 250 K: Frost and co-workers [19,24] used laser-induced fluorescence to detect OH and OD radicals down to 80 and 178 K, respectively, in 2–10 torr of Ar bath gas. These reaction conditions are near the low-pressure limit. Fulle et al. [17] measured this reaction down to 91 K in 750 torr He, where collisional stabilization of HOCO plays an important role. The rate constants measured by the latter group show a slight negative temperature dependence at temperatures below 300 K, exhibiting a maximum around 180 K. The simulations with the modified PES reproduce this trend and predict a more pronounced effect at high temperatures and pressures. On the other hand, calculated reaction rates near the low-pressure limit do not exhibit a clear negative temperature dependence.

The calculated rate constants are in excellent agreement with the experiments of Ravishankara and Thompson [48] and Beno et al. [47] at intermediate temperature range (250–1000 K) and with the shock tube experiments of Wooldridge et al. [22] and Golden et al. [16], as shown in Figs. 2 and 3. Previous kinetic simulations have predicted virtually no temperature dependence of the rate coefficient at low temperatures and pressures [13,17,36], despite the fact that the transition state for dissociation is above the entrance channel. We note that this unusual finding might be the effect of extrapolating three-parameter fits of equilibrium constants measured (or calculated) at higher temperatures (see Appendix).

Pressure Dependence

The pressure dependence of this reaction was studied in a He bath gas up to 3×10^5 torr by a number of investigators [16,17,53–57]. Experimental data, along with our kinetic simulations, are shown in Fig. 4 (at 298 K) and in Fig. 5 (at 250, 400, 500, and 600 K). The simulated falloff curve in He is well reproduced using a value of $\alpha_0 = 150\ \text{cm}^{-1}$, concurring with the value used in the simulations of Ref. [13]. The infinite-pressure limit at 300 K is in agreement with the vibrational relaxation experiments of Brunning and co-workers [34] and Fulle and co-workers [17]. The latter group measured the equilibrium constant for HO + CO association, which results in HOCO intermediates that are 5.5 kcal/mol more stable compared to the PES of Ref. [11]. Interestingly, the heat of formation of HOCO has little impact on the overall kinetics of OH + CO. For instance, if the enthalpy of HOCO is lowered by 5.5 kcal/mol (i.e. that obtained by Fulle et al.), the pressure dependence at 298 K is still well reproduced if α_0 is lowered to 100 cm^{-1}.

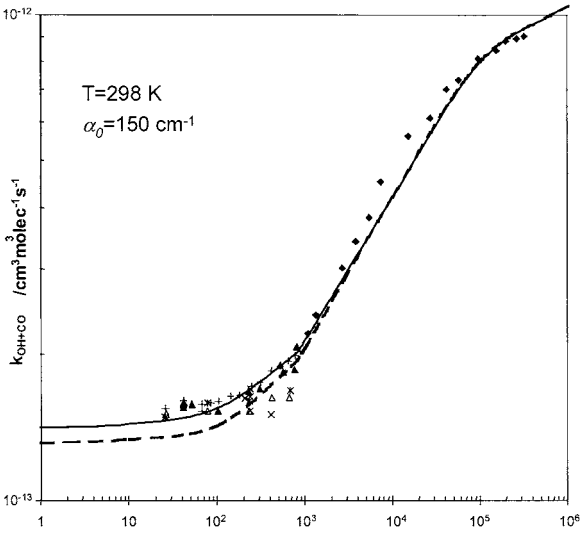

Figure 4 Falloff curve in He bath gas at 298 K. Symbols represent experimental data: + Ref. [16], ◆ Ref. [17], △ Ref. [54], ▲ Ref. [57], × Ref. [55], ✱ Ref. [53]. Lines represent RRKM calculations of present study: He bath gas with ZCT (solid line) and without tunneling corrections (dashed).

At temperatures above 298 K the pressure dependence is well represented with the quoted value of $\alpha_0 = 150\ \text{cm}^{-1}$. However, at 250 K the simulated rate constants are slightly below the experimental numbers, and better agreement is obtained using $\alpha_0 = 180\,\text{cm}^{-1}$. Closer agreement with the experimental falloff curve could be achieved if the energy of TS1 is decreased. Although this causes only a modest increase in the low-pressure rate constant (the rate of HOCO decomposition to the reactants is also enhanced), it results in an overestimation at high pressures.

High-pressure rate coefficients calculated with transition state theory are shown in Fig. 6, along with vibrational relaxation measurements of OH($v = 1$) + CO. The calculated values of k above 300 K are somewhat higher than those observed in vibrational relaxation experiments. *However, we note that the rate constants shown in Fig. 5 at 500 and 600 K, which are clearly not at the high-pressure limit, are also greater than those obtained from vibrational relaxation experiments*. This may be due to the back decomposition of the collision complex to OH($v = 1$) + CO at higher temperatures.

The effect of polyatomic bath gases for the reaction of OH + CO has been studied in air, N_2, CF_4, and SF_6 by several groups [16,52,54,58–60]. It is well known that polyatomics are better energy-quenchers than monoatomic gases, and so the energy transfer parameters, α_0, for SF_6, CF_4, and N_2 are expected to be larger than those of Ar and He. When the pressure-dependent regime was calculated with the

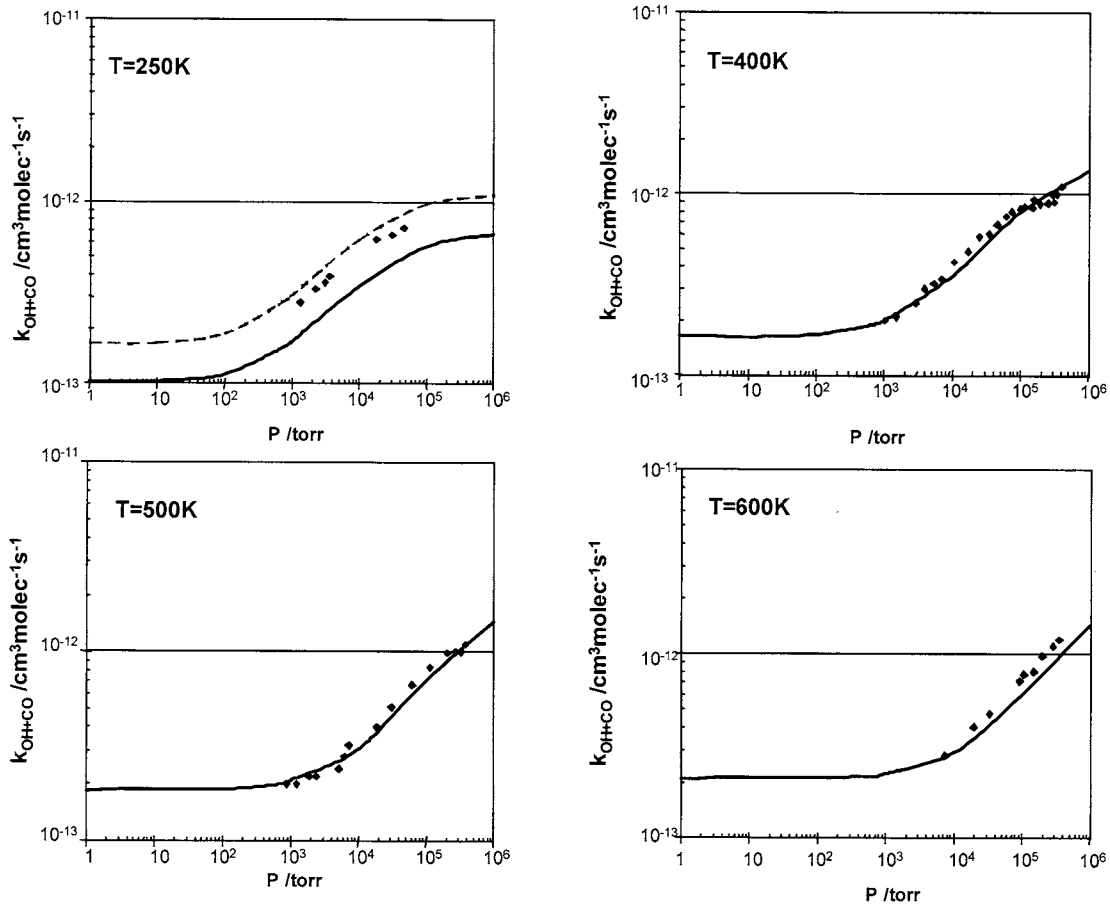

Figure 5 Falloff curves in He bath gas at 250, 400, 500, and 600 K. ◆ Ref. [17]. Solid lines represent simulations in this work with $\alpha_0 = 150$ cm^{-1} (solid lines) and with $\alpha_0 = 180$ cm^{-1} (dashed lines).

aforementioned bath gases, this was indeed found to be the case. The values obtained for α_0 are 800, 680, 300, and 150 cm^{-1} for SF_6, CF_4, N_2, and He, respectively. The calculated rate constants, together with experimental data, are shown in Fig. 7. The values of α_0 used for He is the same as that obtained by other authors [13,17].

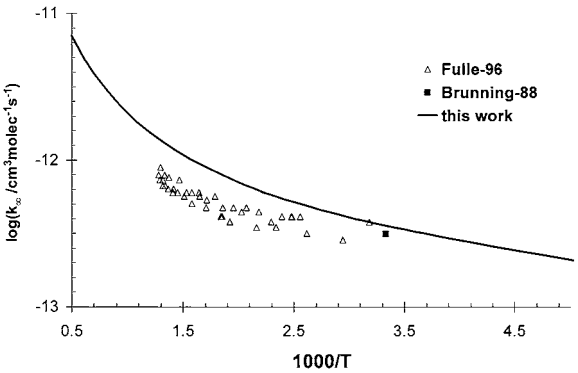

Figure 6 High-pressure rate constants for OH disappearance. Lines represent results obtained in this work using calculated equilibrium constants (solid). Symbols represent experimental determinations: △ Ref. [17], ■ Ref. [34].

Deuterium Effects

Pressure-dependent rate constants for OD + CO have been measured by Paraskevopoulos and Irwin [58] and Golden et al. [16]. The results of our simulations in He, Ar, N_2, CF_4, and SF_6, along with experimental data from these two groups, are shown in Fig. 8. The values of α_0 that best fit the experimental data are 180, 300, 480, 680, and 800 cm^{-1}, respectively. These values are somewhat higher than those of OH + CO for the weaker colliders (i.e. He, Ar, and N_2). [It is possible that the higher barrier of the deuterated reaction (due to differences in zero-point energies) is overpredicted by the PES of Yu et al. (op. cit.) and this is compensated with higher values for the energy transfer parameter.] In contrast with the OH + CO case, the experimental rate constants in Ar are closer to those in He than N_2

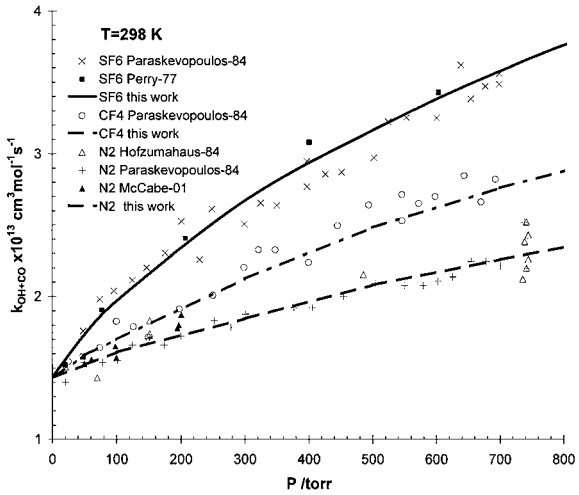

Figure 7 Calculated and experimental pressure-dependent rate constants at 298 K in several bath gases. SF_6 (solid line): present study, × Ref. [59] and ■ Ref. [54]. CF_4 (dashed–dotted line): present study, ○ Ref. [59]. N_2 (dashed line): present study, + Ref. [59], △Ref. [60], ▲ Ref. [57]. The energy transfer parameters, α_0, are 800, 680, and 300 cm^{-1}, respectively.

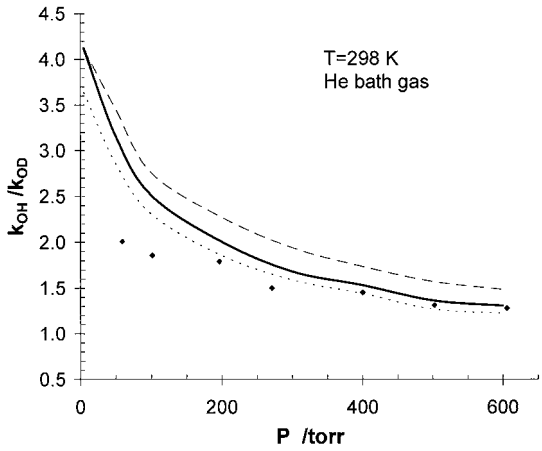

Figure 9 Calculated and observed k_{OH+CO}/k_{OD+CO} ratio at 298 K. Symbols calculated with data from Ref. [16]. Solid line represents calculations presented in this work. Thick line uses a value for α_0 of 150 and 180 cm^{-1} for HOCO and DOCO, respectively; dashed line uses 150 cm^{-1} for both; and dotted line shows effects of scaling the zero-point energies by 0.95.

bath gas, which leads to a relative increase of the energy transfer parameter.

Observed kinetic isotope effects from the data of Ref. [16] are shown in Fig. 9, along with present calculations. The relatively large kinetic isotope effects observed in Fig. 9 can be explained by the increased chemical activation barrier of OD relative to that of OH (the energy of *cis*-TS2 increased from 1.03 to 2.02 kcal/mol because of zero-point corrections).

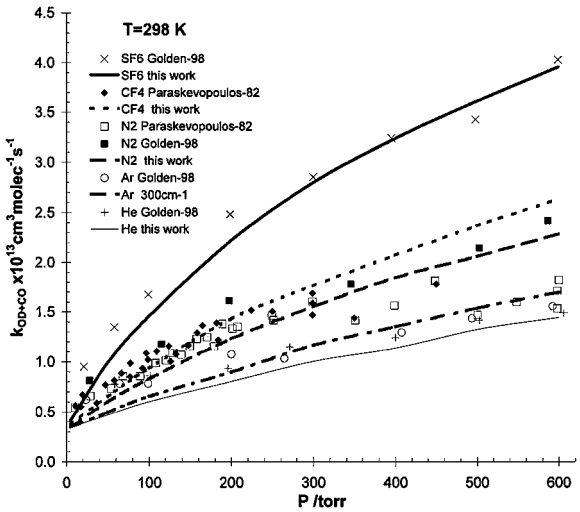

Figure 8 Calculated and experimental pressure-dependent rate constants at 298 K in several bath gases. SF_6 (solid line): this work, × Ref. [16]; CF_4 (short-dashed line): this work, ◆ Ref. [58]. N_2 (long-dashed line): this work, □ Ref. [58], ■ Ref. [16]. Ar (dashed–dotted line): this work, ○ Ref. [16]. He (thin solid line): this work, + Ref. [16]. The energy transfer parameters, α_0, used are 800, 680, 480, 300, and 180 cm^{-1}, respectively.

Quantum Tunneling

Although some authors [13,14,30] have calculated significant barriers for reaction 2, the PES of Yu et al. places the energy of TS2 only 1 kcal/mol above the entrance channel. Since the energy difference between the association and decomposition transition states is quite small (the adjusted energies for *trans*-TS1 and *cis*-TS2 are +0.57 and +0.63 kcal/mol, respectively), the energy range available for tunneling before collisions is quite narrow. Indeed, at 298 K tunneling contributes less than 10% of the total reaction rate, and is negligible in the high-pressure limit. Lowering the energy of TS2 will further diminish the importance of tunneling.

A more detailed treatment of tunneling including multidimensional effects may yield greater transmission probabilities and lead to a flatter Arrhenius curve at low temperatures. However, larger tunneling corrections will result in greater k_{OH+CO}/k_{OD+CO} ratio at low pressures, increasing the difference with observed kinetic isotope effects [16]. Thus, the present calculations indicate that the rate constants below 250 K observed in the experiments of Refs. [17] and [19] are not compatible with higher barriers for reaction 2.

Reaction Modeling and Parametric Expressions

As mentioned earlier, considerable error is introduced when the equilibrium constant for this reaction is expressed with the common three-parameter expression over an extended temperature range ($80 < T/K < 2000$). The same is true when the pressure- and temperature-dependent rate constants are cast into a standard parametric form. For this reason, we provide two sets of parameters, intended for combustion and atmospheric applications. These are shown in Tables II and III, respectively. The values in Table III are in good agreement with the JPL 97-4 data [25] down to 250 K, but are lower then JPL 97-4 by up to 25% at 200 K. In contrast, the rates recommended by IUPAC for atmospheric conditions [53] show slightly negative temperature dependence in this range ($175 < T/K < 300$) and differ from this work by up to factors of 2. The predicted rate coefficients are about 15% higher than the experiments of Refs. [16] and [22] at 2000 K, and this discrepancy is expected to increase if the model is used above this temperature.

CONCLUSIONS

The PES of Ref. [11] is, to the best of our knowledge, the highest level electronic structure calculation performed on this system. The fact that the reaction rate coefficients calculated with this PES tend to underestimate data at room temperature and below is probably an indicator that at least one of the barriers is too high. In order to fit the large body of experimental data available we have fine-tuned this PES by lowering the energy of TS2 by 0.4 kcal/mol. After this adjustment, our model closely reproduces the large body of experiments available at room temperature and above, but slightly underpredicts rates below 250 K. The calculated rate constants can be represented with the parametric expressions in Tables II and III for conditions of interest in combustion modeling and atmospheric chemistry. The latter are in good agreement with the reaction rates recommended in the JPL 97-4 compilation [25]. Perhaps closer agreement with the low-temperature experimental data could be attained if the entropy of TS1 was increased slightly (e.g. by tightening the frequencies) and with a corresponding lowering of its energy. However, vibrational frequencies calculated at the CCSD(T)/cc-pvTZ level (such as those used in Ref. [11]) have been shown to be very accurate, with less than 2% errors [61]. One possible explanation of the apparent rate enhancement at very low temperatures can be a competing mechanism prevailing at low temperatures, possibly involving the stabilization of OHCO and OHOC complexes that form with no apparent energy barrier. These complexes could then isomerize to form energized HOCO intermediates or further react with O_2 producing HO_2 and CO_2.

Table II Optimized Parameters for the Two Channel Rate RRKM/Master Equation Calculations in the $800 < T/K < 2000$ and $0 < P_{N2}/\text{torr} < 10^6$ Range

	a	b	c
CO + OH → HOCO			
K_{eq} [cm^3/(molecule)]	−31.3	1.72	−14,375
k_∞ [cm^3/(molecule s)]	−16.7	1.83	−119
k_0/[M] [cm^6/(molecule s)]	−21.7	−3.85	780
OH + CO → H + CO_2			
k_0 [cm^3/(molecule s)]	−18.8	2.02	−747
$k_\infty \times$ [M] [s^{-1}]	−161.2	51.93	−38,231

$k_i = 10^a T^b \exp(-c/T)$; $K_{eq} = 10^a T^b \exp(-c/T)$; $F_c = 0.60$.

Table III Optimized Parameters for the Two Channel Rate RRKM/Master Equation Calculations in the $175 < T/K < 300$ and $0 < P_{N2}/\text{torr} < 800$ Range

	k_{300}	m
CO + OH → HOCO		
k_∞ [cm^3/(molecule s)]	1.13×10^{-12}	−1.32
k_0/[M] [cm^6/(molecule s)]	5.87×10^{-33}	1.36
OH + CO → H + CO_2		
k_0 [cm^3/(molecule s)]	1.50×10^{-13}	−0.58
$k_\infty \times$ [M] [s^{-1}]	$2.12\text{E} \times 10^{-9}$	−6.08

$k(T) = k(300\text{ K})(\frac{T}{300\text{ K}})^{-m}$; $F_c = 0.6$.

The enthalpy of HOCO is now believed to be somewhat higher than in previous studies. Nonetheless, we find that this has little effect in the global kinetics of OH + CO. In fact, the present model can successfully reproduce experimental rate constants using older values of the HOCO enthalpy and somewhat lower energy transfer parameters.

We found that an extrapolation of a simple three-parameter fit of K_{eq} to temperatures below 170 K (e.g. for interstellar chemistry) introduces considerable error, and gives the appearance of temperature-independent rate coefficient in this range (see Appendix). In contrast to previous findings, our tunneling calculations indicate that the impact of tunneling on the overall rate constant is minor, even at temperatures as low as 80 K. We emphasize that tunneling alone is not sufficient to explain the unusually high rates observed at low temperatures.

APPENDIX

The extrapolation of a three-parameter fit of the equilibrium constant to very low temperatures results in an

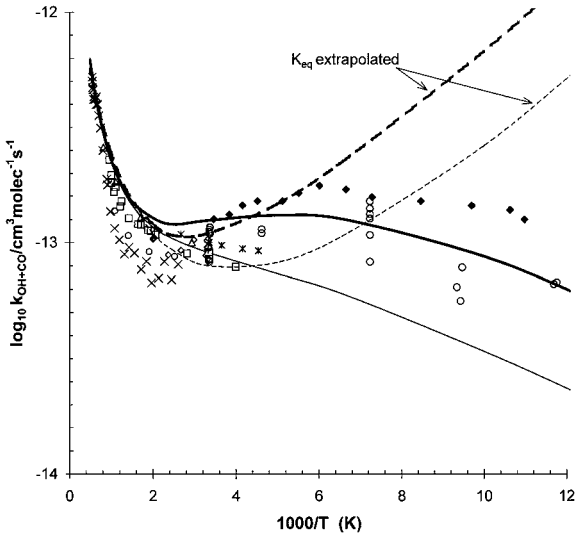

Figure 10 Arrhenius plot of k_{OH+CO} to illustrate the effect of using an extrapolated three-parameter fit for the equilibrium constant. Solid lines are calculations with K_{eq} derived from standard statistical mechanics formulae (see Fig. 2). Dashed lines were calculated using a parametric fit for K_{eq}, fit in the range: $200 < T/K < 2000$ and extrapolated down to 80 K. Thin lines correspond to 10 torr Ar and thick lines to 750 torr He.

unrealistic overestimation of this quantity. This can give the appearance of an enhanced reaction rate at low temperatures that is independent of temperature. Figure 10 illustrates this artifact, with a three-parameter fit in the temperature range $200 < T/K < 2000$. Clearly, a slightly different three-parameter fit could lead to rate constants that appear to be independent of temperatures below 200 K.

The authors are grateful to John Barker for providing the Multiwell code and for his valuable comments.

BIBLIOGRAPHY

1. Ung, A. Y. M.; Back, R. A. Can J Chem Rev Can De Chim 1964, 42, 753–763.
2. Dryer, F. L.; Neageli, D. W.; Glassman, I. Combust Flame 1971, 17, 271–272.
3. Smith, I. W. M.; Zellner, R. J Chem Soc, Faraday Trans II 1973, 69, 1617.
4. Smith, I. W. M. Chem Phys Lett 1977, 49, 112–115.
5. Jacox, M. E. J Chem Phys 1988, 88, 4598–4607.
6. Ruscic, B.; Litorja, M. Chem Phys Lett 2000, 316, 45–50.
7. Ruscic, B.; Schwarz, M.; Berkowitz, J. J Chem Phys 1989, 91, 6780–6785.
8. Scherer, N. F.; Sipes, C.; Bernstein, R. B.; Zewail, A. H. J Chem Phys 1990, 92, 5239–5259.
9. Radford, H. E.; Wei, W.; Sears, T. J. J Chem Phys 1992, 97, 3989–3995; Sears, T. J.; Fawzy, W. M.; Johnson, P. M. J Chem Phys 1992, 97, 3996–4007; Sears, T. J.; Radford, H. E.; Moore, M. A. J Chem Phys 1993, 98, 6624–6631; Petty, J. T.; Moore, C. B. J Chem Phys 1993, 99, 47–55; Petty, J. T.; Harrison, J. A.; Moore, C. B. J Phys Chem 1993, 97, 11194–11198.
10. Ruscic, B.; Wagner, A. F.; Harding, L. B.; Asher, R. L.; Feller, D.; Dixon, D. A.; Peterson, K. A.; Song, Y.; Qian, X. M.; Ng, C. Y.; Liu, J. B.; Chen, W. W. J Phys Chem A 2002, 106, 2727–2747.
11. Yu, H. G.; Muckerman, J. T.; Sears, T. J. Chem Phys Lett 2001, 349, 547–554.
12. Duncan, T. V.; Miller, C. E. J Chem Phys 2000, 113, 5138–5140.
13. Zhu, R. S.; Diau, E. G. W.; Lin, M. C.; Mebel, A. M. J Phys Chem A 2001, 105, 11249–11259.
14. Aoyagi, M.; Kato, S. J Chem Phys 1988, 88, 6409–6418.
15. Kudla, K.; Schatz, G. C.; Wagner, A. F. J Chem Phys 1991, 95, 1635–1647.
16. Golden, D. M.; Smith, G. P.; McEwen, A. B.; Yu, C. L.; Eiteneer, B.; Frenklach, M.; Vaghjiani, G. L.; Ravishankara, A. R.; Tully, F. P. J Phys Chem A 1998, 102, 8598–8606.
17. Fulle, D.; Hamann, H. F.; Hippler, H.; Troe, J. J Chem Phys 1996, 105, 983–1000.
18. NIST, Standard Reference Database—Chemistry Webbook, 2001. http://webbook.nist.gov/chemistry/.
19. Frost, M. J.; Sharkey, P.; Smith, I. W. M. J Phys Chem 1993, 97, 12254–12259.
20. Kudla, K.; Koures, A. G.; Harding, L. B.; Schatz, G. C. J Chem Phys 1992, 96, 7465–7473.
21. Lester, M. I.; Pond, B. V.; Anderson, D. T.; Harding, L. B.; Wagner, A. F. J Chem Phys 2000, 113, 9889–9892; Lester, M. I.; Pond, B. V.; Marshall, M. D.; Anderson, D. T.; Harding, L. B.; Wagner, A. F. Faraday Discuss 2001, 118, 373–385.
22. Wooldridge, M. S.; Hanson, R. K.; Bowman, C. T. Int J Chem Kinet 1994, 26, 389–401.
23. Vandooren, J.; VanTiggelen, P. J.; Pauwels, J. F. Combust Flame 1997, 109, 647–668.
24. Frost, M. J.; Sharkey, P.; Smith, I. W. M. Faraday Discuss 1991, 91, 305–317.
25. DeMore, W. B.; Sander, S. P.; Golden, D. M.; Hampson, R. F.; Kinylo, M. J.; Howard, C. J.; Ravishankara, A. R.; Kolb, C. E.; Molina, M. J. Chemical Kinetics and Photochemical Data for Use in Stratospheric Modeling, NASA-JPL, 1997.
26. Atkinson, R.; Baulch, D. L.; Cox, R. A.; Hampson, R. F.; Kerr, J. A.; Troe, J. J Phys Chem Ref Data 1989, 18, 881–1097; Baulch, D. L.; Cobos, C. J.; Cox, R. A.; Esser, C.; Frank, P.; Just, T.; Kerr, J. A.; Pilling, M. J.; Troe, J.; Walker, R. W.; Warnatz, J. J Phys Chem Ref Data 1992, 21, 411–734.
27. Feller, D.; Huyser, E. S.; Borden, W. T.; Davidson, E. R. J Am Chem Soc 1983, 105, 1459–1466.
28. McLean, A. D.; Ellinger, Y. Chem Phys 1985, 94, 25–41.

29. Bradley, K. S.; Schatz, G. C. J Chem Phys 1997, 106, 8464–8472.
30. Schatz, G. C.; Fitzcharles, M. S.; Harding, L. B. Faraday Discuss Chem Soc 1987, 84, 359–369.
31. Feilberg, K. L.; Billing, G. D.; Johnson, M. S. J Phys Chem A 2001, 105, 11171–11176; Vegiri, A.; Farantos, S. C. Mol Phys 1990, 69, 129–146.
32. Balakrishnan, N.; Billing, G. D. J Chem Phys 1996, 104, 4005–4011; Goldfield, E. M.; Gray, S. K.; Schatz, G. C. J Chem Phys 1995, 102, 8807–8817; Dzegilenko, F. N.; Bowman, J. M. J Chem Phys 1998, 108, 511–518; Dzegilenko, F. N.; Bowman, J. M. J Chem Phys 1996, 105, 2280–2286; Zhang, D. H.; Zhang, J. Z. H. J Chem Phys 1995, 103, 6512–6519.
33. Billing, G. D.; Muckerman, J. T.; Yu, H. G. J Chem Phys 2002, 117, 4755–4760.
34. Brunning, J.; Derbyshire, D. W.; Smith, I. W. M.; Williams, M. D. J Chem Soc, Faraday Trans II 1988, 84, 105–119.
35. Larson, C. W.; Stewart, P. H.; Golden, D. M. Int J Chem Kinet 1988, 20, 27–40; Mozurkewich, M.; Lamb, J. J.; Benson, S. W. J Phys Chem 1984, 88, 6435–6441.
36. Troe, J. In Twenty-Seventh Symposium (International) on Combustion; The Combustion Institute, 1998, p. 167.
37. Stein, S. E.; Rabinovitch, B. S. J Chem Phys 1973, 58, 2438–2445.
38. Barker, J. R.; Yoder, L. M.; King, K. D. J Phys Chem A 2001, 105, 796–809.
39. Barker, J. R. Int J Chem Kinet 2001, 33, 232–245.
40. Guillespie, D. T. J Chem Phys 1977, 81, 2340.
41. Troe, J. J Chem Phys 1977, 66, 4745–4757.
42. Kang, J. K.; Musgrave, C. B.; Senosiain, J. P.; Han, J. H.; Musgrave, C. B.; Golden, D. M. Faraday Discuss 2001, 119, 173–189.
43. Frisch, M. J.; Trucks, G. W.; Schlegel, H. B.; Scuseria, G. E.; Robb, M. A.; Cheeseman, J. R.; Zakrzewski, V. G.; Montgomery, J.; Stratmann, R. E.; Burant, J. C.; Dapprich, S.; Millam, J. M.; Daniels, A. D.; Kudin, K. N.; Strain, M. C.; Farkas, O.; Tomasi, J.; Barone, V.; Cossi, M.; Cammi, R.; Mennucci, B.; Pomelli, C.; Adamo, C.; Clifford, S.; Ochterski, J.; Petersson, G. A.; Ayala, P. Y.; Cui, Q.; Morokuma, K.; Malick, D. K.; Rabuck, A. D.; Raghavachari, K.; Foresman, J. B.; Cioslowski, J.; Ortiz, J. V.; Baboul, A. G.; Stefanov, B. B.; Liu, G.; Liashenko, A.; Piskorz, P.; Komaromi, I.; Gomperts, R.; Martin, R. L.; Fox, D. J.; Keith, T.; Al-Laham, M. A.; Peng, C. Y.; Nanayakkara, A.; Challacombe, M.; Gill, P. M. W.; Johnson, B.; Chen, W.; Wong, M. W.; Andres, J. L.; González, C.; Head-Gordon, M.; Replogle, E. S.; Pople, J. A. Gaussian 98 Computer Program, Revision A.7; Gaussian Inc., Pittsburgh, PA, 1998.
44. Truhlar, D. G.; Isaacson, A. D.; Garrett, B. C. In Generalized Transition State Theory; Baer, M. (Ed.); CRC Press: Boca Raton, FL, 1985; Vol. IV, p. 65.
45. González, C. A.; Allison, T. C.; Louis, F. J Phys Chem A 2001, 105, 11034–11040.
46. Miller, W. H. J Am Chem Soc 1979, 101, 6810–6814.
47. Beno, M. F.; Jonah, C. D.; Mulac, W. A. Int J Chem Kinet 1985, 17, 1091–1101.
48. Ravishankara, A. R.; Thompson, R. L. Chem Phys Lett 1983, 99, 377–381.
49. Westenberg, A. A.; deHaas, N. J. J Chem Phys 1973, 58, 4061–4065.
50. Greiner, N. R. J Chem Phys 1969, 51, 5049–5051.
51. Davis, D. D.; Fischer, S.; Schiff, R. J Chem Phys 1974, 61, 2213–2219.
52. Hynes, A. J.; Wine, P. H.; Ravishankara, A. R. J Geophys Res [Atmos] 1986, 91, 1815–1820.
53. Atkinson, R.; Baulch, D. L.; Cox, R. A.; Hampson, R. F.; Kerr, J. A.; Rossi, M. J.; Troe, J. J Phys Chem Ref Data 1997, 26, 521–1011.
54. Perry, R. A.; Atkinson, R.; Pitts, J. N. J Chem Phys 1977, 67, 5577–5584.
55. DeMore, W. B. Int J Chem Kinet 1984, 16, 1187–1200.
56. Forster, R.; Frost, M.; Fulle, D.; Hamann, H. F.; Hippler, H.; Schlepegrell, A.; Troe, J. J Chem Phys 1995, 103, 2949–2958.
57. McCabe, D. C.; Gierczak, T.; Talukdar, R. K.; Ravishankara, A. R. Geophys Res Lett 2001, 28, 3135–3138.
58. Paraskevopoulos, G.; Irwin, R. S. Chem Phys Lett 1982, 93, 138–143.
59. Paraskevopoulos, G.; Irwin, R. S. J Chem Phys 1984, 80, 259–266.
60. Hofzumahaus, A.; Stuhl, F. Phys Chem Chem Phys 1984, 88, 557–561.
61. Galabov, B.; Yamaguchi, Y.; Remington, R. B.; Schaefer, H. F. J Phys Chem A 2002, 106, 819–832.